Effect of vegetative canopy architecture on vertical transport of massless particles

Brian N. Bailey[a], Rob Stoll[a,*], Eric R. Pardyjak[a], Walter F. Mahaffee[b]

[a] *Department of Mechanical Engineering, University of Utah, Salt Lake City, UT, USA*
[b] *U. S. Department of Agriculture - Agricultural Research Service, Horticulture Crops Research Laboratory, Corvallis, OR, USA*

Abstract

Large-eddy simulations of approximately resolved heterogeneous vegetative canopies with repeating row structure were compared to 'equivalent' homogeneous simulations to explore how overall canopy density and horizontal heterogeneity influence the vertical transport of non-depositing massless fluid parcels. A Lagrangian approach was used to quantify particle dispersion. The subgrid component of particle motion was modeled with a Langevin equation that was integrated with a new semi-implicit scheme that successfully minimized rogue trajectories. With rogue trajectories controlled, the subgrid model had a negligible impact on average statistics. Analysis suggested that above the canopy top, canopy density and heterogeneity had a minor effect on mean profiles of particle concentration and vertical flux. However, increasing canopy density resulted in a linear increase in particle residence time, and increased the importance of release height on canopy escape. The average time of persistent vertical particle motions did not follow this monotonic trend. For sufficiently dense canopies, the time scale of persistent vertical motions increased with decreasing canopy density in agreement with mixing-layer scaling. As wall shear became significant, a transition was observed in which persistence decreased with decreasing canopy density. The effect of canopy heterogeneity on residence time and persistence was well correlated with the strength of dispersive fluxes. Canopy heterogeneity

*Corresponding author
Email address: rstoll@eng.utah.edu (Rob Stoll)

decreased the average time for a particle to escape the canopy, and also reduced the coherence of vertical particle motions.

Keywords: Lagrangian particle dispersion model, Large-eddy simulation, Persistence time, Residence time, Sparse canopy, Vineyard

1. Introduction

Understanding the mechanisms that influence airborne transport of particulate matter (e.g., pollutants, allergens, water droplets, microorganisms) is critical for many atmospheric applications. The majority of particles entrained in the atmosphere originate at Earth's surface, which is dominated by plant canopies (Morris and Kinkel, 2002). Thus, understanding the impact of plant canopies on particle transport is essential in a wide range of urban, agronomic, and forestry applications. These applications include vegetative windbreaks designed to mitigate fugitive dust which has a negative impact on human health (Davidson et al., 2005), limiting unwanted cross-pollination in agricultural systems (Hoyle and Cresswell, 2007), and the turbulent transport of plant pathogens which is the primary means by which many disease epidemics spread within plant communities (McCartney et al., 2006).

Canopy flows are generally characterized by strong flow heterogeneity, intermittency, and non-Gaussian flow statistics that limit the applicability of simplified modeling approaches (Poggi et al., 2006). It is believed that the mechanism responsible for these complexities is the presence of mixing-layer-like vortical structures produced by a shear instability at the canopy top (Raupach et al., 1996). Since these intermittent structures are highly efficient at transporting scalars (e.g., pollutants, temperature, moisture) even in the presence of low gradients, understanding the dynamics of these structures appears critical to describe particle transport in canopies.

Most of our understanding of particle transport in canopies is based on dispersion in dense, horizontally homogeneous canopies. Scalar transport in complex canopies remains an open research question (Belcher et al., 2012). Previ-

ous research has demonstrated an important connection between the specifics of canopy architecture and momentum dynamics (e.g., Poggi et al., 2004; Bailey and Stoll, 2013). Bailey and Stoll (2013) reported that plant spacing and foliage density can dramatically impact vertical momentum transport locally, and hypothesized that these areas of high vertical momentum flux may have a substantial impact on particle transport. Prior work has also suggested important links between canopy density and particle dispersion (e.g., Endalew et al., 2011; Thistle et al., 2011). Most man-made vegetation structures (e.g., crops, windbreaks, forest clearings) have substantial heterogeneity at the plant scale that can potentially play an important role in how scalars disperse. This makes understanding these links a critical part of developing new and useful canopy management strategies, as well as gaining insight into how heterogeneous terrain interacts with particulates suspended in the air above.

The present study characterizes the effects of canopy geometry on particle transport. Previous work on this subject generally relies on intuitive and qualitative predictions of how dispersion should change as canopy density is varied (e.g., Pace, 2005). However, a systematic study quantifying these trends does not currently exist. We seek to quantify the impact of canopy architecture on the structure of the turbulent flow and how particles disperse vertically from their source. This was done by simulating dispersion of massless, non-depositing particles in various row-oriented canopies in which row geometry is explicitly resolved. These resolved canopy simulations are contrasted with analogous horizontally homogeneous canopies to examine the importance of horizontal heterogeneity.

2. Numerical Models

The various models that have been applied to canopy dispersion all make compromises between physical description and computational cost. Large-eddy simulation (LES) is a popular technique that sacrifices some computational cost in order to approximately resolve the temporal and spatial features of the most

energetic turbulent scales of motion. In LES, turbulent scales larger than the numerical grid dimension Δ (resolved scales) are directly obtained by solving the relevant governing equations, while scales below Δ (unresolved scales) are modeled. This method is ideally suited for modeling canopy flows in which spatial and temporal details of the flow are important.

For flows where the dispersion of particulates is of interest, it is common to use an LES momentum field to drive a Lagrangian particle dispersion model (LPDM) (e.g., Weil et al., 2004; Wei et al., 2006; Bohrer et al., 2008). LPDMs calculate particle trajectories in a Lagrangian frame of reference based on information about the Eulerian flowfield. Viewing dispersion in a Lagrangian framework naturally lends itself to problems where source location or details about particle trajectories may be important.

2.1. Momentum solution

A complete description of the numerical models used to simulate momentum transport in this study can be found in Stoll and Porté-Agel (2006) and Bailey and Stoll (2013). Essential modeling details are presented below.

Here, the LES technique is used to obtain instantaneous realizations of the velocity field $\widetilde{u}_i$ for turbulent length scales larger than the characteristic grid dimension Δ, where $\widetilde{u}_i$ denotes the filtered velocity component in each Cartesian direction ($1 = x$ = streamwise, $2 = y$ = spanwise, $3 = z$ = vertical). The SGS stress term is calculated using the Smagorinsky model, where the Smagorinsky coefficient, C_s, is calculated dynamically along fluid particle trajectories following Stoll and Porté-Agel (2006). Test filtering for the scale-dependent SGS closure scheme is performed at scales of 2Δ and 4Δ, where $\Delta = (\Delta_x \Delta_y \Delta_z)^{1/3}$. Drag forces of individual canopy elements are aggregated over a grid cell following Shaw and Schumann (1992). The computational domain of size $L_x \times L_y \times L_z$ is discretized into uniform grid cells of size $\Delta_x \times \Delta_y \times \Delta_z$.

The domain for the momentum solution is periodic in the horizontal directions and is driven using a spatially uniform streamwise pressure gradient. The upper boundary consists of a zero-flux rigid lid. The bottom boundary surface

is a stationary no-slip wall, which is enforced by specifying the shear stress at the lowest computational level using Monin-Obukhov similarity theory locally at every boundary point at every time iteration (Stoll and Porté-Agel, 2006). Thermal effects have been neglected for simplicity, as these effects are not the focus of this study. Viscous and rotational (Coriolis) forces are assumed to be negligible at the length scales studied here.

Presented statistics are temporally averaged over the longest available statistically steady period of the simulation (denoted by an overbar). A horizontal average is denoted by $\langle\cdot\rangle$, and a deviation from this average is denoted by $''$.

2.2. Lagrangian dispersion model

Scalar transport is simulated by calculating the trajectories of a large number of "marked" material points or fluid particles. For simplicity, this study focuses on passive particles with zero mass and drag that do not become deposited on surfaces within the domain.

Given a position $x_{p,i}$ of each particle at time $t = t_o$, trajectories can be calculated at some later time $t = t_o + \Delta t_p$ according to

$$x_{p,i}(t_o + \Delta t_p) = x_{p,i}(t_o) + \int_{t_o}^{t_o+\Delta t_p} (u_{r,i} + u_{s,i})\ \mathrm{d}t, \tag{1}$$

where $u_{r,i}+u_{s,i} = u_{L,i}$ is the total velocity of the fluid particle. $u_{r,i}\,\mathrm{d}t$ represents the component of particle motion due to resolved motion, which is known from the LES solution assuming that $\tilde{u}_i = u_{r,i}$ at the particle location $x_{p,i}$. The component $u_{s,i}\,\mathrm{d}t$ represents particle motion due to unresolved scales which must be modeled.

The unresolved particle velocity $u_{s,i}$ was modeled analogous to Weil et al. (2004). It was assumed that the Langevin equation and Gaussian probability density function (PDF) given by Thomson (1987) for velocity fluctuations about the ensemble mean also hold for SGS velocity fluctuations. It is important to note that this approach only assumes that SGS velocity fluctuations are Gaussian. The PDF of resolved velocity fluctuations is not specified a priori, a distinct advantage over ensemble particle transport approaches. Using this

assumption and the further assumption that the SGS stress tensor is isotropic (Weil et al., 2004), an equation for the evolution of the SGS particle velocity can be written as

$$\mathrm{d}u_{s,i} = -\frac{u_{s,i}}{T_{Ls}}\mathrm{d}t + \frac{1}{2}\left(\frac{1}{\sigma_s^2}\frac{\mathrm{d}\sigma_s^2}{\mathrm{d}t}u_{s,i} + \frac{\partial\sigma_s^2}{\partial x_i}\right)\mathrm{d}t + \left(\frac{2\sigma_s^2}{T_{Ls}}\right)^{1/2}\mathrm{d}\xi_i, \qquad (2)$$

where the material derivative is defined as $\mathrm{d}/\mathrm{d}t = \partial/\partial t + \partial/\partial x_k\,(u_{r,k} + u_{s,k})$, $\sigma_s^2 = 2/3e_s$ where e_s is the SGS turbulent kinetic energy (*tke*), $\mathrm{d}\xi_i$ is a component of Gaussian white noise with zero mean and variance of $\mathrm{d}t$, and T_{Ls} is the SGS Lagrangian time scale which was chosen to be equal to the time scale from the Lagrangian averaging procedure used to calculate the SGS stress tensor τ_{ij}. For the chosen τ_{ij} model, this is the most logical choice for T_{Ls} since this is the Lagrangian timescale for the sub-grid scales. Any other choice for T_{Ls} would be inconsistent with sub-grid behavior of the momentum field. However, this may not be the case for other codes adopting different τ_{ij} models. T_{Ls} depends on the grid scale, nonlinear SGS transport, and the magnitude of the SGS shear stress (see Meneveau et al., 1996; Stoll and Porté-Agel, 2006). This previous work has shown that a T_{Ls} that varies with this collection of parameters behaves as expected when shear or grid resolution are varied.

The SGS *tke* is estimated using a combination of the SGS length and velocity scales as $e_s = \left(\Delta C_s|\tilde{S}|\right)^2/0.3$, with $|\tilde{S}|$ given by $\left(2\tilde{S}_{ij}\tilde{S}_{ij}\right)^{1/2}$ and $\tilde{S}_{ij} = \frac{1}{2}\left(\frac{\partial\tilde{u}_i}{\partial x_j} + \frac{\partial\tilde{u}_j}{\partial x_i}\right)$. For the flows and grid resolution considered in this study, using an anisotropic version of Eq. 2 instead of the isotropic model had no impact on results. The isotropic model was also shown to perform well in a highly convective boundary layer by Weil et al. (2004). However, in flows with larger shear (i.e., off-diagonals of $\tilde{S_{ij}}$) or simulations using coarser grid resolution, it is possible that SGS stress anisotropy may have an impact on particle motion.

Equation 2 was integrated using a new semi-implicit numerical scheme that was designed to reduce non-physical or 'rogue' trajectories, which became problematic when a simple forward Euler scheme was used (see Appendix A).

All Eulerian quantities needed for the Lagrangian dispersion model are in-

terpolated from the grid nodes to the particle position using trilinear interpolation. Below the lowest computational grid point, the resolved velocities at particle locations were obtained by linear extrapolation to zero at the aerodynamic roughness height z_o. For particles that traveled beyond horizontal boundaries, trajectories were calculated using periodicity of the flow field, such that horizontal particle positions always remained on the interval $x_1 \in [0, L_x)$ and $x_2 \in [0, L_y)$. At the top and bottom boundaries, the particles implicitly follow the momentum field zero flux condition since they are passive fluid parcels driven by the momentum field. Instances where particles did not satisfy the zero-flux condition were due to numerical errors caused either by the model for $u_{s,i}$ or by discretization errors in time or space. In the extremely rare event that a particle traveled below $z = z_o$ or above $z = L_z$, the particle was reflected according to a perfectly elastic collision. The particle timestep was chosen such that particles adhered to the Courant stability condition (i.e., a particle cannot traverse more than one Eulerian grid cell in a single timestep), which guarantees that the timestep is much smaller than the Lagrangian integral scale. This timestep may not be small enough to prevent rogue trajectories in the SGS dispersion model. A discussion of this issue and our remedy is presented in Appendix A.

3. Simulation Details

The simulation cases used in this study are a sub-set of those presented in Bailey and Stoll (2013). Essential details of the simulated canopies and model inputs are reproduced below.

3.1. Canopy geometries

Canopy geometry was varied by altering the spatial distribution of the leaf area density (LAD). The plant canopy chosen in this study is a trellis-trained crop (e.g., a grapevine canopy) with mean flow perpendicular to the row direction. The rows are infinitely long in the spanwise direction, and repeat

indefinitely in the streamwise direction. Row geometry is resolved by specifying the LAD as a square wave along streamwise transects. For a further description of numerical representation of the canopy see Bailey and Stoll (2013).

Individual rows have leaf area index (LAI) values of 1.0 and 3.0, and row spacings (r_s) range from 1.0 to 6.0 m. A complete list of canopy geometries is given in Table 1. The row height and width were set to $h = 2.0$ m and $r_w = 0.5$ m, respectively. The drag coefficient was chosen to have a constant value of $c_d = 0.5$ to eliminate the effects of the spatial distribution and functional form of the drag coefficient, as they are not a focus of this study.

To characterize the effects of canopy heterogeneity, 'equivalent density' horizontally homogeneous canopies were simulated for each of the row-resolved canopy geometries. The LAIs of the horizontally homogeneous canopies were specified such that they were equivalent to the row-resolved geometries when integrated over whole-canopy scales. The effective LAI was defined as

$$\overline{LAI} = LAI\left(\frac{\mathcal{V}_r}{\mathcal{V}_t}\right) = LAI\left(\frac{r_w}{r_w + r_s}\right), \tag{3}$$

where $\mathcal{V}_r/\mathcal{V}_t$ is the volume occupied by vegetation ($\mathcal{V}_r$) per unit volume of canopy ($\mathcal{V}_t$).

Following Bailey and Stoll (2013), simulations are named according to the convention of [R/H]LAI.r_s, where [R/H] takes the value of R for row-resolved geometries or H for horizontally homogeneous geometries. For example, the row-resolved case of $LAI = 3.0$ and $r_s = 1.0$ m is denoted by R3.1. Simulation nomenclature is also given for reference in Table 1.

3.2. Simulation inputs

The LES model's simulated domain was set to $L_x \times L_y \times L_z = 24h \times 24h \times 8h$, which was discretized onto a uniform grid of $192 \times 192 \times 160$ points. The streamwise pressure gradient responsible for driving the flow was chosen to be $F_x = 0.025$ m s^{-2}. The aerodynamic roughness length was given a value of $z_o = 0.005$ m.

Particles were released continuously from a uniform grid of point sources located within the canopy ($z \leq h$). The grid of release locations consisted of five equispaced vertical release heights within the canopy ($z_r\, h^{-1} = 0.2$, 0.4, 0.6, 0.8, and 1.0) and five equispaced spanwise point sources. Streamwise release locations were specified such that there were four uniformly spaced point sources per row period. This was done to test the impact of particle release position with respect to the rows. Particle statistics showed no sensitivity to horizontal release location, and therefore results in Sect. 4 are presented as an average over all horizontal point source locations at a given height. Since the number of release locations was allowed to vary with row spacing, the release rate from each point source was varied across cases to maintain a constant overall release rate of 10^3 particles s^{-1} for the entire canopy. This equates to a release rate of $Q = 0.087$ particles s^{-1} m^{-2} at each of the five release heights. Over the course of each simulation, a total of 10^6 particles were released. This value was chosen such that releasing more particles had a minimal effect on results. The release locations for the horizontally homogeneous canopies were given the same values as their corresponding row-resolved geometry counterparts. The time step used in the integration of Eq. 2 was given a constant value of approximately $\Delta t_p = 0.04h\, u_*^{-1}$.

4. Results

4.1. Momentum field validation

To validate how well the model is able to reproduce reality, simulated wind profiles were compared with profiles obtained from the field experiment of Miller et al. (2014). The experiment was conducted in a grapevine canopy (*Vitis vinifera*) in Oregon, USA (44° 49' 2" N 123° 14' 17" W). The row cross-sections measured approximately $r_w \times h = 0.5{\times}1.9$ m^2, and were spaced at $r_s = 2.0$ m. The row LAI was measured using destructive methods, and was found to be 7.5. The wind velocity vector was measured at 20 Hz using a vertical array of four sonic anemometers (Campbell Scientific, Logan, UT). The experimental

canopy was simulated by creating a new (row-resolved) case that reflected the geometry described above.

Profiles of first- and second-order velocity moments are compared for the simulated and experimental canopies in Fig. 1 (a single prime denotes a departure from the time average). Within the canopy, simulated results show good agreement with measurements. Above the canopy streamwise velocity moments were under predicted, which was likely a result of the top boundary condition. We found that increasing domain height continually improved agreement with measurements from the upper sonics. Bailey and Stoll (2013) demonstrated that increasing domain height had a minimal effect on near-canopy profiles and flow structures, and therefore we feel that an increase in domain height for the present study does not appear necessary.

4.2. Lagrangian time scales and impacts of SGS particle motion

It is important to establish the relative contribution of SGS motions to overall particle transport. This can be evaluated by comparing the resolved and SGS Lagrangian time scales. Eulerian approximations of the Lagrangian time scales are convenient to use because they are easier to calculate and interpret. This means that we can evaluate the vertical locations at which SGS contributions may be important. The resolved Lagrangian time scale can be estimated from Eulerian quantities by assuming isotropy and using Kolmogorov's similarity theory as follows (Rodean, 1996)

$$T_{Lr} = \frac{2\sigma_{ave}^2}{C_0 \varepsilon}, \tag{4}$$

where $\sigma_{ave}^2 = \left(\tilde{\sigma}_u^2 + \tilde{\sigma}_v^2 + \tilde{\sigma}_w^2\right)/3$ is the average of the three components of the resolved velocity variance, C_0 is a universal constant taken here to be 4.0 (Thomson, 1987), and ε is the viscous dissipation rate. The viscous dissipation rate was estimated using the relation $\varepsilon \approx \Pi = -\tau_{ij}\tilde{S}_{ij}$, which holds on average assuming that Δ is in the inertial subrange. The SGS Lagrangian time scale reported in this section is the time scale previously introduced in Eq. 2.

Ideally, the resolved Lagrangian time scale should be much larger than the SGS time scale. If this is the case, particle motion is dominated by resolved motions and SGS particle model choice becomes unimportant. The inverse of the SGS and resolved components of the Lagrangian timescale (Figs. 2a and 2b) are combined to form the ratio of the resolved to SGS Lagrangian time scales (Fig 2c). Note that the inverse time scale is reported so that large values correspond to regions of the flow that are less resolved. The timescale ratio shows that the resolved time scale is at least two orders of magnitude larger than the SGS time scale, indicating that the flow is well-resolved by the numerical grid. This is not surprising considering that the dominant scales of motion in canopy flows are thought to be on the order of the canopy height (Finnigan, 2000), which is much larger than the grid scale Δ.

To verify that the Eulerian estimates were indeed reasonable, the Lagrangian time scales were also calculated directly by integrating the autocorrelation function of the resolved and SGS velocity magnitudes (Fig. 3). Release height had relatively little effect on the Lagrangian time scales, and therefore averages over all release heights are presented. The SGS timescale was several times smaller when calculated from particle trajectories. This is likely due to influence from the additional terms in Eq. 2 that do not scale linearly with $T_{L,s}$. Regardless of this difference, both the Eulerian and Lagrangian methods for calculating the SGS time scale resulted in similar importance of SGS motions. To confirm these conclusions, particle dispersion statistics were computed assuming $u_{si} = 0$. We found that SGS particle model choice had no noticeable impact on the trends in dispersion statistics for the cases considered here, and all conclusions presented in this paper can be made whether or not a model for u_{si} was used.

4.3. Dispersion profiles

4.3.1. Particle concentrations

Profiles of particle concentration are given in Fig. 4 for various release heights. Concentrations are calculated as described in Flesch et al. (1995). It is important to keep in mind that lateral boundary conditions are periodic, and

therefore the concentration profiles include particles at all distances from the source. As a result, the profiles reflect near-source distributions as well as well-mixed particles far downstream. Additionally, since there is no vegetation or ground deposition, particles are allowed to build up near the wall and continue without ever becoming deposited.

Concentration profiles demonstrate that as overall canopy density is increased particle concentrations increase, particularly near the release height. This result is expected since denser canopy elements slow vertical mixing (Thistle et al., 2011). In the upper canopy particle concentrations were relatively insensitive to canopy density and release height. Concentrations in the lower canopy were much more sensitive to release height. An increase in concentration of about 20% was found between the sparsest and densest cases for the lowest release. For downstream distances near the source the effects of release height are amplified, as concentration distributions have not yet become well mixed (not shown). Far above the canopy, profiles are well-mixed regardless of canopy geometry. The apparent discontinuity in the concentration profiles at $z = \Delta_z$ is a consequence of the fact that flow is not resolved below Δ_z. Concentrations linearly approach zero at $z = z_o$ below Δ_z, as flow variables are also linearly interpolated to zero at $z = z_o$.

Analogous to mean velocity profiles, canopy heterogeneity also had a minimal impact on the shape of normalized mean concentration profiles.

4.3.2. Vertical particle fluxes

Vertical flux profiles (Fig. 4) were calculated as described in Aylor and Flesch (2001). The expected trend is observed for an elevated area source, which is a net upward flux above the source and a net downward flux below the source. There is a net negative (counter-gradient) flux below the source, which is increasingly significant as release height is increased. Since there is no source for particles below the release height, it is impossible to have a net positive flux below the release height since any particle that travels downward after release must either remain below the source or return back upward. This means that

there is a net storage of particles below the release height, which indicates that particles transported downward after release are transported back above the release height at a slower rate. Asymmetric vertical transport corresponds to the commonly observed dominance of sweep events over ejection events in the canopy (Finnigan, 2000; Bailey and Stoll, 2013), and motivates the idea that particles tend to become trapped in the lower canopy. As the release height approaches the wall, the negative flux below the release height is negligible and the maximum F_z/Q approaches 1.0 which indicates no storage below.

Canopy geometry had an overall minimal impact on particle flux profiles. The slope of the flux profile increases slightly near the source for the densest case, which indicates decreased transport away from the source. This corresponds to higher near-source concentrations.

4.4. Persistence time

Previous work has often reported that turbulent motions in canopy flows have a high degree of organization or structure (Finnigan, 2000). A statistic termed 'persistence time' is a useful measure of coherence, which was first applied to canopy flow by Chamecki (2013). The persistence time is defined more generally as the average amount of consecutive time that some variable ϕ spends above or below a threshold value $\mathcal{T}$ (Fig. 5). The time of individual persistence events can be averaged together to form the mean persistence time above the threshold (t^+) and below the threshold (t^-). The nomenclature $t^{+/-}(\phi, \mathcal{T})$ is introduced to denote the persistence time of variable ϕ for a given threshold $\mathcal{T}$. A notable advantage of the persistence time over the more traditional integral timescale is that it allows the distinction between upward and downward transport events.

4.4.1. Persistence of the vertical particle velocity

The study of Chamecki (2013) used persistence time to examine coherence in plant canopy flows using the Eulerian vertical velocity, which concluded that upward persistence events lasted up to twice as long as downward events. We ex-

amine persistence in the more natural Lagrangian framework, where the statistic is calculated along particle pathlines (Fig. 6). Thus it captures coherent motions that begin at a certain level and proceed to traverse different levels of the flow. We set the persistence variable ϕ_L (subscript L denoting a Lagrangian quantity) to vertical particle velocity (w_L) and the threshold is given a value of zero, which means $t^{+/-}(w_L, 0)$ is the persistence of upward and downward particle motions.

Unlike the Eulerian analysis of Chamecki (2013), we found that the persistence time for upward and downward events were roughly equivalent. This suggests that although at a given level in the canopy sublayer upward events are more persistent, as the particle changes levels the potential for upward versus downward transport equalizes.

For the homogeneous canopies the persistence time remains relatively constant for $\overline{LAI} \geq 0.6$ and increases between $0.3 \leq \overline{LAI} \leq 0.6$. This increase is likely due to the fact that the dominant length scale near the canopy increases as a function of canopy-top shear (Raupach et al., 1996). A further reduction in canopy density results in an abrupt decrease in persistence time. This suggests a transition in the organization of the flow around $\overline{LAI} = 0.3$. Interestingly, this is the point at which the wall shear stress begins to become significant (see Bailey and Stoll, 2013). As the canopy becomes sparse and wall shear begins to dominate, it is expected that decreasing canopy density should lead to increased stress and therefore lower persistence.

The introduction of canopy heterogeneity decreased persistence times. These decreases were largest in cases with large row LAI and spacing. Bailey and Stoll (2013) showed that these cases also generated the largest dispersive fluxes, which are fluxes induced by mean flow heterogeneity. It is likely that increased within-canopy stresses contribute to a reduction in the coherence of particle motions, resulting in lower persistence times. It is also possible that mean streamline displacements in the Eulerian momentum field disrupt particle motions as they are diverted around individual canopy elements. However, it is unclear how the canopy elements affect an individual particle's trajectory as streamline dis-

placements are not visible in the instantaneous Eulerian flowfield. Persistence is decreased for all cases except R3.3, which is not surprising as R3.3 has negligible dispersive fluxes and mean streamline displacements.

Release height had an effect on vertical velocity persistence times in some cases. Lower release heights showed decreased downward persistence times, whereas the opposite was true for upward persistence times. It follows logically that particles released lower within the canopy should have lower potential for downward persistence, as they will eventually reach the wall. Likewise, particles released lower in the canopy show increased upward persistence time. Although these effects of release height are relatively minimal, it is expected that they will be amplified if only particles near their source are considered, as particles will inevitably lose 'memory' of their release location as time progresses.

The SGS particle velocity model choice did have some effect on persistence times. Not including the effects of SGS particle motions resulted in a nearly uniform increase in persistence times, while general trends remained the same. It follows logically that the addition of pseudo-random small-scale fluctuations should generally decrease persistence.

4.5. Residence time

An important variable that quantifies canopy escape by particles is residence time. Particle residence time is defined here as the amount of consecutive time after release that a particle remains below either the trunk or canopy height. Since trunks are not explicitly resolved, an arbitrary height of $z = 0.5h$ was chosen to be the height of the trunk-space, which is roughly based on the LAD profile.

Normalized canopy residence times for the trunk-space and canopy-space (Fig. 7) were in the range of 2.0-9.0, which is consistent with values reported by Fuentes et al. (2007) and Edburg et al. (2012).

For near canopy-top releases, canopy residence times were small and showed little variation with change in canopy density. This agrees with mean particle concentration profiles (Fig. 4) which showed that the integrated amount of

particles within the canopy had little dependence on canopy geometry for upper canopy releases.

Release height had a substantial impact on residence time, which increased with increasing canopy density. For the lowest release height ($z_r = 0.2h$), trunk-space and canopy residence times nearly doubled between the sparsest and densest canopies. Residence times varied by a factor of almost three amongst all release heights in the H1.6 case, and by a factor of almost five in the H3.1 case. This is evidence that release height plays a stronger role in canopy escape in denser canopies due to a stronger disconnect between the upper and lower canopy.

The dependence of residence time on overall canopy density was found to be approximately linear for the homogeneous canopies, which can be expressed by the general function $T_R\, u_*/h = \alpha\, \overline{LAI} + \beta$, where α and β are functions of release height. Values of α and β are tabulated for the homogeneous cases in Table 2. Linear fits were generally very good, except when the release height was near the canopy top where there was minimal variation in residence time with canopy density.

Canopy heterogeneity had the effect of decreasing residence times. Cases that showed significant reductions in residence times were those that had the largest dispersive fluxes. These reductions caused the residence time to diverge from the linear relationship with $\overline{LAI}$ for the homogeneous cases. Heterogeneity had the largest impact in the R3.6/H3.6 case, which also has the largest dispersive fluxes (Bailey and Stoll, 2013). In this case, the introduction of heterogeneity resulted in a roughly 20% reduction in both trunk-space and canopy residence times. This is almost certainly due to some combination of increased penetration of turbulence structures and increased streamline displacements characteristic of cases with large row LAI and spacing.

5. Summary

The impact of plant canopy architecture on particle dispersion was studied by comparing a series of simulations in which canopy heterogeneity was approximately resolved to corresponding 'equivalent' density homogeneous canopies. The present study builds on the momentum transport study of Bailey and Stoll (2013) by adding a particle dispersion component, with focus directed toward vertical particle transport. Particles were released from point sources at various heights and horizontal locations within the canopy and tracked in a Lagrangian frame of reference, which provided highly detailed information about particle trajectories.

Model choice for unresolved particle motions did not have a significant effect on bulk particle dispersion statistics as long as a scheme was used to minimize unphysical or 'rogue' trajectories that are associated with integration of the equation for unresolved particle velocities. For this purpose, a new semi-implicit fractional step integration scheme was developed that substantially reduced rogue trajectories when compared to a simple forward Euler scheme.

Mean particle concentrations within the canopy showed expected behavior and increased with increasing canopy density, particularly near the release height. This was especially true for lower canopy releases. Increased particle concentrations corresponded to decreased vertical flux divergence near the release height. Overall, concentration and vertical flux profile shapes were dominated by the release height, while the effect of canopy heterogeneity was minimal.

The vertical persistence time (Chamecki, 2013) was applied in a Lagrangian framework, providing a measure of the coherence of vertical particle motions. Results indicated that as canopy density was decreased, persistence times were constant or increased until a critical point, at which a sharp decrease was observed. This transition happened at approximately $\overline{LAI} = 0.3$, and corresponded to similar transitions in streamwise velocity statistics. It was hypothesized that this transition was a result of non-zero wall stresses creating

increased variance. There was a range of homogeneous canopies in which persistence reached a constant value ($\overline{LAI} \geq 0.6$) which could indicate that for sufficiently dense canopies persistence becomes constant, although further work is required to confirm this speculation. The presence of canopy heterogeneity decreased persistence times in cases with significant dispersive fluxes. This was attributed to the discontinuous nature of canopy elements, which decreased the overall coherence of the flow.

Increasing canopy density caused particles to reside below the canopy top longer after release due to decreased fluxes and turbulence structure penetration. Increasing release height decreased particle residence time, as particles released lower within the canopy will naturally take longer to be transported above the canopy top. The addition of canopy heterogeneity reduced particle residence times in some cases due to increased turbulence structure penetration. Using this information, a simple linear model was developed to describe residence time in a homogeneous canopy.

While particle deposition onto plant elements was not considered in this study, it is expected that residence time will play a role on deposition rates. Pardyjak et al. (2008) formulated a deposition efficiency time scale, T_*, which represents the ratio of the residence time scale to the time after release until deposition. The study demonstrated decreasing importance of deposition with decreasing foliage density, as indicated by increased deposition time scales. Future work on this subject should include examining the effects of canopy density on deposition, which could be used to develop parameterizations for bulk deposition velocities for use in canopy transport models.

Acknowledgments

This research was supported by National Science Foundation (NSF) grants IDR CBET-PDM 113458, EPS 1208732, and AGS 1255662 and United States Department of Agriculture (USDA) project 5358-22000-039-00D. We would like to acknowledge high-performance computing support from Yellowstone (ark:/85065/d7wd3xhc)

provided by NCAR's Computational and Information Systems Laboratory, sponsored by the NSF. An allocation of computer time from the Center for High Performance Computing at the University of Utah is also gratefully acknowledged. The use, trade, firm, or corporation names in this publication are for information and convenience of the reader. Such use does not constitute an endorsement or approval by the NSF, USDA, and the Agricultural Research Service of any product or service to the exclusion of others that may be suitable.

Appendix A. Semi-implicit fractional-step time integration scheme

Numerical integration of the generalized Langevin equation proposed by Thomson (1987) gives rise to unstable modes that can often result in unrealistic or 'rogue' particle trajectories, particularly when a simple forward Euler scheme is used (Yee and Wilson, 2007). Wilson (2012) suggested that the problem may be cured simply through a sufficient reduction in the time step, although such a reduction is usually not feasible in complex flows.

We found that rogue trajectories resulting from unphysical SGS velocities became problematic if no measures were taken to control them. This effect was amplified as canopy density was decreased. For practical purposes, a rogue trajectory was defined as any particle that traversed more than one computational grid cell during a single time step, or $\tilde{u}_{Li} + u_{si} > \Delta_i/\Delta t_p$. Aside from the fact that rogue trajectories (as defined here) lead to a violation of the Courant stability condition, they also caused a substantial fraction of particles to be ejected out the top of the domain, which should not happen. Aggressive *ad hoc* intervention was required to control rogue trajectories, which lead to serious questions about the degree to which the well-mixed condition and SGS model were adversely affected. The semi-analytical integration scheme of Yee and Wilson (2007) was implemented in an attempt to reduce rogue trajectories. However, we found that the conditions necessary to obtain the analytical solution were very frequently not satisfied, which often led to *ad hoc* intervention.

Instead, a semi-implicit time integration scheme was developed to solve

Eq. 2. This scheme used a fractional step method to separate the numerical integration of Eq. 2, where two sub-steps are integrated using simple implicit and forward Euler schemes, respectively. Using this scheme, rogue trajectories became highly infrequent and occurred only about every 50,000 particle updates, as opposed to every few hundred updates when the forward Euler scheme alone was used.

Analogous to Yee and Wilson (2007), the integration is separated into substeps that isolate the linear and non-linear terms. However, rather than performing the first integration step analytically, a simple implicit scheme was used as follows

$$u^*_{s,i} = u^0_{s,i} - \frac{u^*_{s,i}}{T_{Ls}}\mathrm{d}t + \frac{1}{2}\left(\frac{1}{\sigma_s^2}\left[\frac{\partial\sigma_s^2}{\partial t} + \frac{\partial\sigma_s^2}{\partial x_j}u_{r,j}\right]u^*_{s,i} + \frac{\partial\sigma_s^2}{\partial x_i}\right)\mathrm{d}t + \left(\frac{2\sigma_s^2}{T_{Ls}}\right)^{1/2}\mathrm{d}\xi_i, \tag{A.1a}$$

$$u_{s,i} = u^*_{s,i} + \frac{1}{2}\frac{1}{\sigma_s^2}\frac{\partial\sigma_s^2}{\partial x_j}u^*_{s,j}u^*_{s,i}\mathrm{d}t. \tag{A.1b}$$

Beginning with some particle velocity $u^0_{s,i}$ at time $t = t_0$, $u^*_{s,i}$ can be determined from Eq. A.1a algebraically, as the linear nature of this equation means that each velocity component is decoupled. In cases where τ_{ij} is not diagonal, the linear integration step can be computed by solving a 3×3 linear system of equations for $u^*_{s,i}$. Given the intermediate velocity values (u^*_{si}), the velocity at time $t + \Delta t_p$ can be determined from Eq. A.1b. The non-linear sub-step cannot be solved implicitly, and therefore a forward Euler step is used. This scheme is not dynamically stable, and will occasionally result in rogue trajectories. However, simulations indicated that these events were very rare. In the unlikely case that the scheme produced a rogue trajectory, this sub-step was skipped.

References

Aylor, D.E., Flesch, T.K., 2001. Estimating spore release rates using a Lagrangian stochastic simulation model. J. Appl. Meteorol. 40, 1196–1208.

Bailey, B.N., Stoll, R., 2013. Turbulence in sparse organized vegetative canopies: A large-eddy simulation study. Boundary-Layer Meteorol. 147, 369–400.

Belcher, S.E., Harman, I.N., Finnigan, J.J., 2012. The wind in the willows: Flows in forest canopies in complex terrain. Ann. Rev. Fluid Mech. 44, 479–504.

Bohrer, G., Katul, G.G., Nathan, R., Walko, R.L., Avissar, R., 2008. Effects of canopy heterogeneity, seed abscission and inertial on wind-driven dispersal kernels of tree seeds. J. Ecol. 96, 569–580.

Chamecki, M., 2013. Persistence of velocity fluctuations in non-Gaussian turbulence within and above plant canopies. Phys. Fluids 25, 115110.

Davidson, C.I., Phalen, R.R., Solomon, P.A., 2005. Airborne particulate matter and human health: a review. Aerosol Sci. Technol. 39, 737–749.

Edburg, S.L., Stock, D., Lamb, B.K., Patton, E.G., 2012. The effect of the vertical source distribution on scalar statistics within and above a forest canopy. Boundary-Layer Meteorol. 142, 365–382.

Endalew, A.M., Debaer, C., Rutten, N., Vercammen, J., Delele, M.A., Ramon, H., Nicola i, B.M., Verboven, P., 2011. Modelling the effect of tree foliage on sprayer airflow in orchards. Boundary-Layer Meteorol. 138, 139–162.

Finnigan, J.J., 2000. Turbulence in plant canopies. Ann. Rev. Fluid Mech. 32, 519–571.

Flesch, T.K., Wilson, J.D., Yee, E., 1995. Backward-time Lagrangian stochastic dispersion models and their application to estimate gaseous emissions. J. Appl. Meteorol. 34, 1320–1332.

Fuentes, J.D., Wang., D., Bowling, D.R., Potosnak, M., Monson, R.K., Goliff, W.S., Stockwell, W.R., 2007. Biogenic hydrocarbon chemistry within and above a mixed deciduous forest. J. Atmos. Chem. 56, 165–185.

Hoyle, M., Cresswell, J.E., 2007. The effect of wind direction on cross-pollination in wind-pollinated GM crops. Ecol. Appl. 17, 1234–1243.

McCartney, H., Fitt, B., West, J., 2006. Dispersal of foliar plant pathogens: mechanisms, gradients and spatial patterns, in: Cooke, B.M., Jones, D.G., Kaye, B. (Eds.), The Epidemiology of Plant Diseases. Springer, pp. 159–192.

Meneveau, C., Lund, T.S., Cabot, W.H., 1996. A Lagrangian dynamic subgrid-scale model of turbulence. J. Fluid Mech. 319, 353–385.

Miller, N.E., Stoll, R., Mahaffee, W., Neill, T.M., Pardyjak, E., 2014. An experimental study of momentum and heavy particle transport in a trellised agricultural canopy. Submitted for review to Agric. For. Meteorol.

Morris, C.E., Kinkel, L.L., 2002. Fifty years of phyllosphere microbiology: significant contributions to research in related fields, in: Lindow, S.E., Hecht-Poinar, E.I., Elliott, V.J. (Eds.), Phyllosphere microbiology. APS Press, St. Paul, USA, pp. 365–375.

Pace, T.G., 2005. Methodology to Estimate the Transportable Fraction (TF) of Fugitive Dust Emissions for urban Scale Air Quality Analyses. Technical Report. U. S. EPA.

Pardyjak, E.R., Speckart, S.O., Yin, F., Veranth, J.M., 2008. Near source deposition of vehicle generated fugitive dust on vegetation and buildings: Model development and theory. Atmos. Environ. 42, 6442–6452.

Poggi, D., Katul, G.G., Albertson, J.D., 2006. Scalar dispersion within a model canopy: Measurements and three-dimensional Lagrangian models. Adv. Water Res. 29, 326–335.

Poggi, D., Porporato, A., Ridolfi, L., Albertson, J.D., Katul, G.G., 2004. The effect of vegetation density on canopy sub-layer turbulence. Boundary-Layer Meteorol. 111, 565–587.

Raupach, M.R., Finnigan, J.J., Brunet, Y., 1996. Coherent eddies and turbulence in vegetation canopies: the mixing-layer analogy. Boundary-Layer Meteorol. 78, 351–382.

Rodean, H.C., 1996. Stochastic Lagrangian Models of Turbulent Diffusion. Amer. Meteor. Soc., Boston, MA. 84 pp.

Shaw, R.H., Schumann, U., 1992. Large-eddy simulation of turbulent flow above and within a forest. Boundary-Layer Meteorol. 61, 47–64.

Stoll, R., Porté-Agel, F., 2006. Dynamic subgrid-scale models for momentum and scalar fluxes in large-eddy simulations of neutrally stratified atmospheric boundary layers over heterogeneous terrain. Water Resources Res. 42, W01409.

Thistle, H.W., Strom, B., Strand, T., Peterson, H.G., Lamb, B.K., Edburg, S., Allwine, G., 2011. Atmospheric dispersion from a point source in four Southern pine thinning scenarios: basic relationships and case studies. T. ASABE 54, 1219–1236.

Thomson, D.J., 1987. Criteria for the selection of stochastic models of particle trajectories in turbulent flows. J. Fluid Mech. 180, 529–556.

Wei, G., Vinkovic, I., Shao, L., Simoëns, S., 2006. Scalar dispersion in large-eddy simulation and a Lagrangian stochastic subrid model. Phys. Fluids 18, 095101.

Weil, J.C., Sullivan, P.P., Patton, E.G., 2004. The use of large-eddy simulations in Lagrangian particle dispersion models. J. Atmos. Sci. 61, 2877–2887.

Wilson, J.D., 2012. “Rogue velocities” in a Lagrangian stochastic model for idealized inhomogeneous turbulence, in: Lin, J., Brunner, D., Gerbig, C., Stohl,

A., Luhar, A., Webley, P. (Eds.), Lagrangian Modeling of the Atmosphere. American Geophysical Union, Washington, DC, pp. 53–57.

Yee, E., Wilson, J.D., 2007. Instability in Lagrangian stochastic trajectory models, and a method for its cure. Boundary-Layer Meteorol. 122, 243–261.

Table 1: Vineyard geometry cases and their respective labels and effective leaf area indexes.

Row-resolved			Homogeneous	
LAI	r_s (m)	Case	$\overline{LAI}$	Case
3.0	1.0	R3.1	1.000	H3.1
3.0	2.0	R3.2	0.600	H3.2
3.0	6.0	R3.6	0.230	H3.6
1.0	1.0	R1.1	0.333	H1.1
1.0	6.0	R1.6	0.077	H1.6

Table 2: Linear regression coefficients for normalized particle residence time, as defined by $T_R\, u_*/h = \alpha\, \overline{LAI} + \beta$. Coefficients are given for the homogeneous canopy cases for each release height. Goodness of fit is quantified by the coefficient of determination, R^2.

trunk-space				canopy-space			
z_r/h	α	β	R^2	z_r/h	α	β	R^2
0.2	2.33	3.03	0.99	0.2	3.94	4.85	0.98
0.4	1.04	1.71	0.94	0.4	2.70	3.60	0.96
				0.6	1.23	2.90	0.90
				0.8	0.19	2.27	0.31

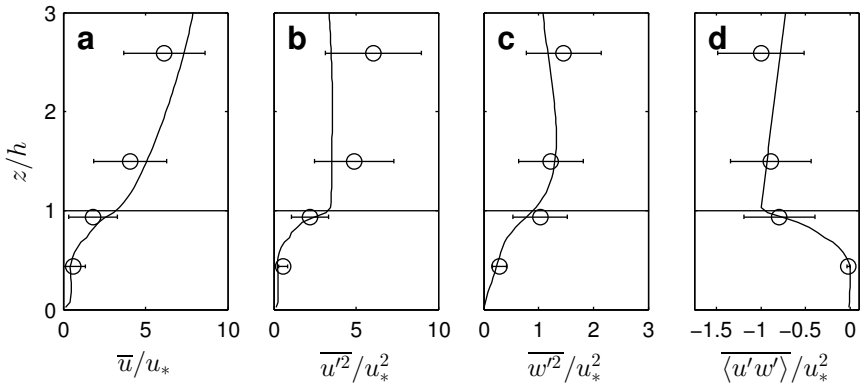

Figure 1: Velocity moment profiles for simulated (solid lines) and experimental (open circles) canopies. (a) mean velocity, (b) streamwise velocity variance, (c) vertical velocity variance, (d) vertical momentum flux. Error bars denote ± 1 standard deviation from the mean value.

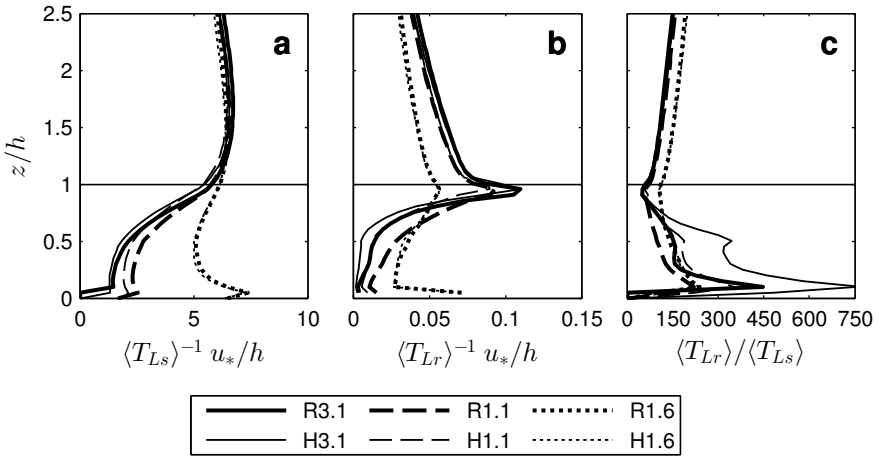

Figure 2: Profiles of (a) plane averaged inverse of the SGS Lagrangian time scale $\langle T_{Ls}^{-1}\rangle$, (b) plane averaged inverse of the resolved Lagrangian time scale $\langle T_{Lr}^{-1}\rangle$, and (c) the ratio of SGS to resolved Lagrangian time scales $\langle T_{Lr}\rangle/\langle T_{Ls}\rangle$. Lagrangian time scales were calculated through Eulerian approximations.

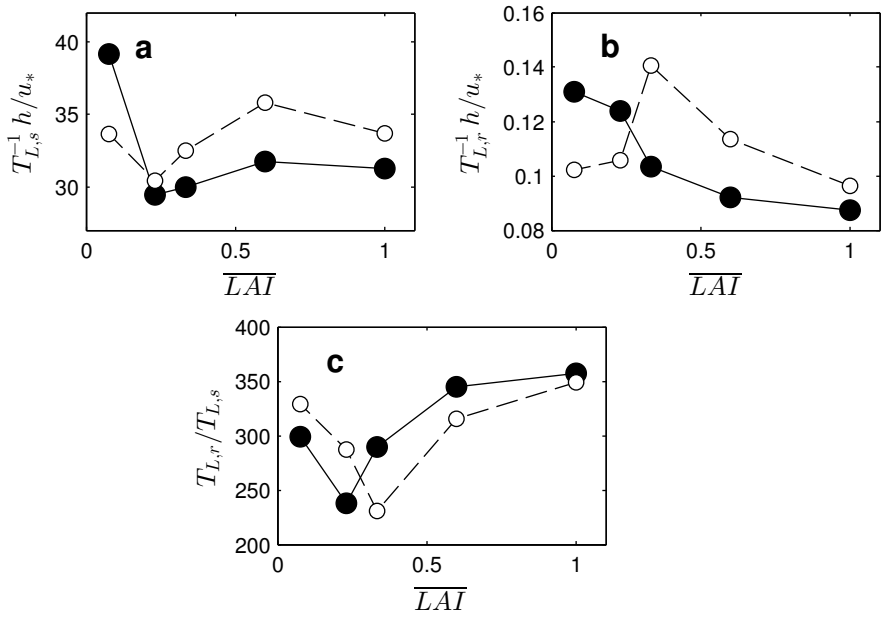

Figure 3: Variation with overall canopy density of the (a) inverse of the SGS Lagrangian time scale, (b) inverse of the resolved Lagrangian time scale, and (c) ratio of SGS to resolved Lagrangian time scales. Dashed lines with open markers denote homogeneous canopy cases, while solid lines with filled markers denote row-resolved cases. Lagrangian time scales were calculated directly from particle trajectories.

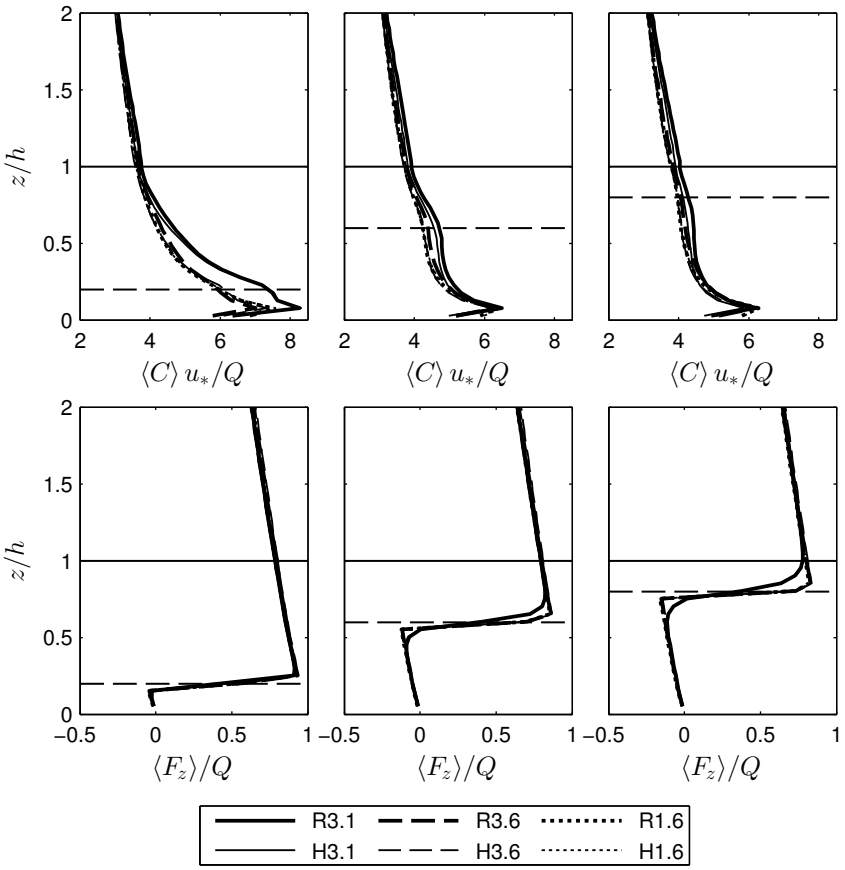

Figure 4: Row 1 shows profiles of normalized particle concentration, and row 2 shows profiles of normalized vertical particle flux. Columns correspond to varying release height (denoted by a horizontal dashed line at $z = z_r$).

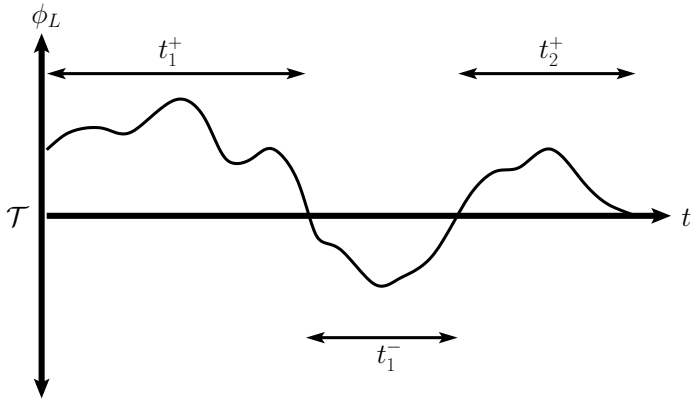

Figure 5: Illustration of individual persistence times from a typical time-series, which is used to calculate the mean persistence time. The mean persistence time, $t^{+/-}$, is the mean of each of the individual persistence events $t_n^{+/-}$.

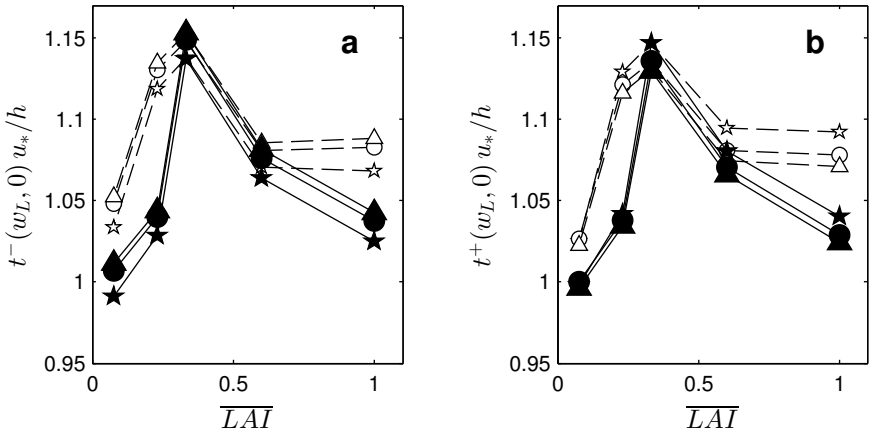

Figure 6: Mean persistence time of vertical particle velocity (a) less than zero (b) greater than zero. Solid lines with filled markers denote row-resolved cases, while dashed lines with open markers denote homogeneous canopies. Marker type denotes release height: $z_r = 0.2h$ (★); $z_r = 0.6h$ (●); $z_r = h$ (▲)

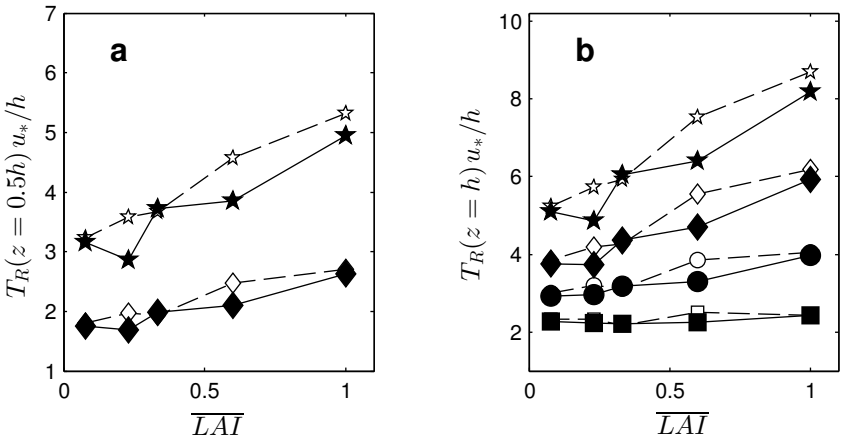

Figure 7: Mean particle residence time within (a) the trunk-space ($z \leq 0.5h$) and (b) the canopy-space ($z \leq h$), which is defined as the average time after release it takes a particle to escape the trunk/canopy space. Solid lines with filled markers denote row-resolved cases, while dashed lines with open markers denote homogeneous cases. Marker type denotes release height: $z_r = 0.2h$ (★); $z_r = 0.4h$ (⧫); $z_r = 0.6h$ (●); $z_r = 0.8h$ (■)